Interactions between brush-coated clay sheets in a polymer matrix

Rong Wang, Feng Qiu,[a] Hongdong Zhang, and Yuliang Yang
Department of Macromolecular Science, The Key Laboratory of Molecular Engineering of Polymers, Ministry of Education, China and Fudan University, Shanghai, 200433 China

(Received 7 October 2002; accepted 26 February 2003)

The interactions between clay sheets with lateral length L that are grafted by polymer chains of N monomers immersed in a chemically identical polymer melt of polymerization index P are calculated by using Edwards' self-consistent field theory. The calculation is carried out in two dimensions and shows that, as expected, for short grafted chains ($aN^{1/2} \ll L$, with a the segment size), the interactions and concentration profiles of the grafted layers are that of stretched brushes at flat interface; while for long grafted chains ($aN^{1/2} \gg L$), the interactions and concentration profiles are characteristic of star polymers. In the practically useful (but analytically untractable) case of intermediate grafted chain lengths, where $aN^{1/2} \sim L$, we have found that the lateral length of the clay sheets is a new relevant length scale in determining the structure and interactions of the grafted layers. These results indicate that the structure and interactions of the brush-coated clay sheets can be tailored by varying the grafted chain length and/or the lateral length of the clay sheets to benefit the fabrication of polymer/clay nanocomposites. © *2003 American Institute of Physics.*
[DOI: 10.1063/1.1568339]

I. INTRODUCTION

Polymeric nanocomposites are composed of polymers and dispersed inorganic particles with at least one dimension at nanoscale.[1] Examples include adding the inorganic clay montmorillonite to nylon-6,[2] reinforcing polypropylene by particulates fibers, and layered inorganic fillers,[3] confining poly(ethylene oxide) in parallelly stacked montmorillonite layers,[4] and incorporating graphitic oxide and clays into conducting polymers, such as polyaniline and polypyrrole.[5,6] Such composites may exhibit dramatic increases in tensile strength, heat resistance, optical clarity, barrier properties, scratch resistance, and flame retardancy. It is now generally understood that for polymeric nanocomposites to achieve these improved properties the inorganic particles have to be molecularly dispersed within the polymer matrix. In practice, however, the van der Vaals interactions between the inorganic particles are always attractive, which result in the aggregation or flocculation of the particles. It is, thus, important to tailor the surfaces of the particles to control the surface force. One common means is to end-graft polymer chains onto the particle surfaces, forming what is usually referred to as a *polymer brush.* These brushes are of both practical and theoretical interest and have been the subject of intense study since the pioneering work of Alexander[7] and de Gennes.[8]

When a polymer brush is immersed in a polymer melt, the osmotic effects tend to swell the brush, while the elasticity of the grafted chains tends to diminish the brush extension. The balance of the two effects results in an equilibrium brush height, which depends on three parameters, the polymerization indexes of the grafted chains, N, and the melt chains, P, as well as the grafting density σ (average number of grafted chains per surface area a^2 of the solid substrate, where a is the monomer size). For long enough polymer melt chains, i.e., $P \gtrsim N^{1/2}$, the bare monomer–monomer interactions of the N chains often described by an excluded-volume parameter, are screened out by the P chains, and the N chains behave ideally.[9] When the grafting density is low, $\sigma N^{1/2} \ll 1$, the free melt polymer chains penetrate the brush (''wet brush'') and the brush height scales as $h \simeq aN^{1/2}$; where the grafting density is high enough, $\sigma N^{1/2} \gg 1$, the melt chains are completely expelled from the brush (''dry brush'') and its height scales as $h \simeq aN\sigma$.[10] The interface between the brush and the melt, however, is not sharp; the melt penetrates over a distance λ inside the brush. This phenomenon arises as a balance between two effects. On the one hand, penetrating the brush is entropically favorable for the solvent; on the other hand, the melt penetration implies an extra stretching of the chains in the outer fringe of the brush and a subsequent cost in elastic free energy. The penetration length λ was calculated by Leibler *et al.* for a melt of long chains: $\lambda = a\sigma^{-1/3}N^{1/2}$ for $P > P^* = N^{2/3}\sigma^{-2/3}$, i.e., $\sigma N^{1/2} > (N/P)^{3/2}$.[11] In this regime, the melt wets the brush only partially and there exists a positive interfacial energy between the grafted chains of the brush and the mobile chains of the bulk. In the case of short melt molecules ($P < P^*$), Leibler *et al.* predicted complete wetting and the penetration length scales as $\lambda = a\sigma^{-1}NP^{-1}$ for $P < P^* = N^{2/3}\sigma^{-2/3}$.[11,12]

Although the scaling analyses were rather successful in giving qualitative prediction and interpretation of experimental observations, they were limited in providing detailed information about the specific density profiles and interactions of the polymer brush/melt systems. Using a continuous one-dimensional self-consistent field (SCF) theory, Ferreira *et al.* performed a systematic exploration of the parameter space of

[a]Author to whom correspondence should be addressed. Electronic mail: fengqiu@fudan.edu.cn

a polymer protected surface in contact with a melt.[13] Their calculation shows that due to subtle entropic effects the melt chains are expelled from the grafted layer, even if they are chemically identical to the grafted chains, and the interactions between the clay sheets can be purely repulsive or repulsive at short distances and attractive at longer distances. The domain where attraction exists between two grafted layers, and where partial wetting is thus expected, can be simply described by $\sigma N^{1/2} > (N/P)^2$, which is slightly different from the just described scaling prediction, $\sigma N^{1/2} > (N/P)^{3/2}$. Combining the Scheutjens and Fleer SCF method and an analytical SCF theory, Balazs *et al.* recently investigated the interactions between two closely spaced surfaces and the surrounding polymer melt, in which short chains (surfactants) are terminally anchored to each of the surfaces.[14] Their calculations show that adding a small fraction of end-functionalized polymers to the melt can lead to the formation of exfoliated structures, where the sheets are uniformly dispersed within the matrix. These results reveal that the optimal polymeric candidates for creating stable exfoliated composites are those that would constitute optimal steric stabilizers for colloidal suspensions.

In all the previous theoretical studies the clay sheets were assumed to be so big that their lateral lengths are much longer than the size scale of the grafted polymers. Therefore, all of the existing studies are in one dimension and their argument is valid only for very long sheets ($L \gg aN^{1/2}$). These assumptions are apparently inadequate for nano-sheets, where the inorganic clays (montmorillonite being a prime example) consist of stacked silicate sheets, each sheet is approximately 200 nm in length and 1 nm in thickness.[2] For a ''dry'' polymer brush with index of polymerization equal to 1000, segment length 0.2 nm, and grafting density 0.5, the brush height is approximately 100 nm, which is the same order as the lateral length of the sheets. However, such regimes with intermediate sheet length, which is important to applications of nano-sheets, have entirely been left out by the previous theoretical studies. Attempting to deal with this practically useful case of intermediate sheet lengths, here we report numerical calculations that do not impose any assumption on the sheet length. We use the SCF formulism originally developed by Edwards and extended to multicomponent mixtures by Hong and Noolandi to investigate the morphologies and interaction potentials of the brush-coated clay sheets/polymer melt system.[15–19]

II. MODEL

We consider a system of two parallel clay sheets with a distance H along the x-axis and grafted with n_α polymer chains of polymerization index N (Fig. 1). The two sheets are immersed in a polymer matrix of n_β free chains with polymerization index P. To simplify the calculation, we assume that the lateral length of the sheets in the y-axis is much larger than the brush height. Thus, due to the translational invariance along the y-axis, the calculation can be reduced to two dimensions and the clay sheets are represented by two parallel $L \times W$ rectangles in the xz-plane, where L and W are the lateral length along the z-axis and the thickness of the clay sheets, respectively. The surfaces of the clay sheets are

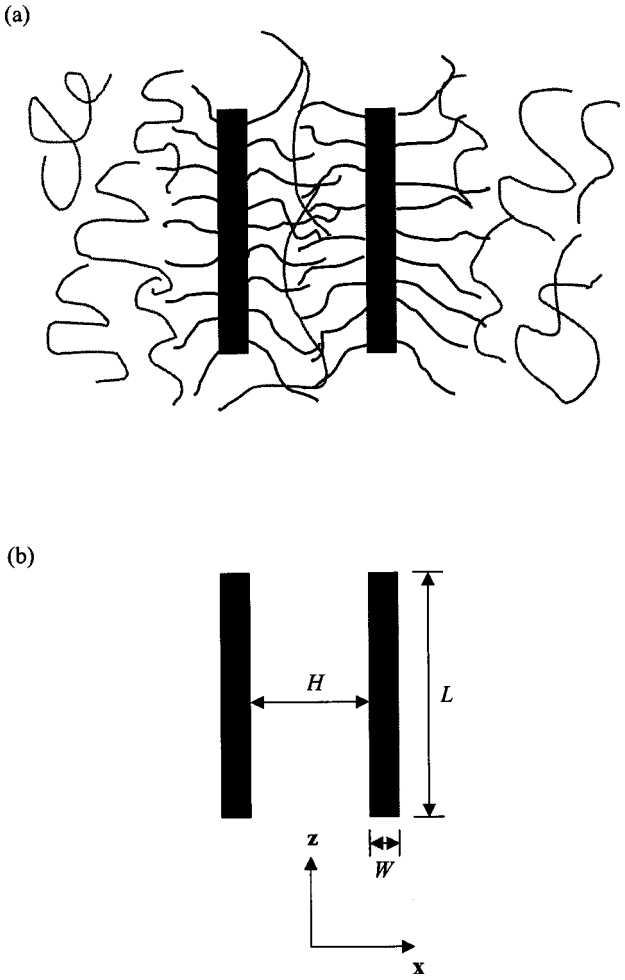

FIG. 1. (a) 2D schematic diagram of the geometry of two brush-coated clay sheets in a polymer melt. The long lateral length along the y-axis is much larger than the brush height, thus only a cross section in the xz-plane is drawn. The two clay sheets are represented by two rectangles and the grafted chains are drawn darker than the melt chains. Note that the x-direction is perpendicular to the surfaces of the clay sheets. (b) Schematic diagram illustrating the variables used in the calculation. Note that H is the distance between the two front surfaces of the clay sheets.

denoted as $\mathbf{r}_c$. At sufficiently large distance away from the sheets, the influence of the brushes ceases to exist and the P melt chains attain their bulk properties. The bulk is characterized by a constant mean density of monomers $\psi_0 = 1$. The monomers of the grafted chains and the free chains are assumed to be chemically identical, flexible with a statistical length a, and incompressible with a volume ρ_0^{-1}. The volume occupied by the polymers is $V = (n_\alpha N + n_\beta P)\rho_0^{-1}$ and the grafting density of the grafted chains is $\sigma = an_\alpha/4(L + W)$, which is dimensionless and defined as the average number of grafted chains per surface area a^2 of the solid substrate, where a is the monomer size. It should be noted that this definition of σ implies that n_α and n_β are actually the number of (grafted and matrix) polymers contained in a box of dimension $L_x \times L_z \times a$, where L_x, L_z, and a are the system sizes along the x, z and y-axes, respectively. The average volume fraction of the grafted chains is defined as $\bar{\psi}_\alpha = n_\alpha N \rho_0^{-1}/V$ and that of the matrix chains $\bar{\psi}_\beta = n_\beta P \rho_0^{-1}/V$.

The system we considered here consists of many interacting chains. In general, a many interacting system is not analytically tractable and a variety of approximations has to be taken, in which the mean field approximation is a good first step to go. In the mean field theory the many interacting chains are reduced to that of independent chains subject to an external (mean) field, created by the other chains. The fundamental quantity to be calculated in mean field studies is the polymer segment probability distribution function, $q(\mathbf{r},s)$, representing the probability of finding segment s at position $\mathbf{r}$. The probability, $q_\alpha(\mathbf{r},s)$, that a grafted chain ends at $\mathbf{r}$ in s steps having started at the surfaces of the clay sheets satisfies a modified diffusion equation

$$\frac{\partial q_\alpha(\mathbf{r},s)}{\partial s}=\frac{a^2}{6}\nabla^2 q_\alpha(\mathbf{r},s)-w_\alpha(\mathbf{r})q_\alpha(\mathbf{r},s), \tag{1}$$

where $w_\alpha(\mathbf{r})$ is the self-consistent field, the initial condition, $q_\alpha(\mathbf{r}=\mathbf{r}_c,0)=1$ and $q_\alpha(\mathbf{r}\neq\mathbf{r}_c,0)=0$, and the boundary condition is $q_\alpha(\mathbf{r}=\mathbf{r}_c,s)=0$. To implement these conditions without contradictions, the trick introduced by Dolan and Edwards was adopted.[20] Because the two ends of the grafted chains are distinct, a second end-segment distribution function, $q_\alpha^\dagger(\mathbf{r},s)$, is needed. It satisfies Eq. (1) with the right-hand side multiplied by -1, and the initial condition, $q_\alpha^\dagger(\mathbf{r},N)=1$, and the boundary condition, $q_\alpha^\dagger(\mathbf{r}=\mathbf{r}_c,s)=0$.

For the free chains (β chains), the two ends are identical, therefore, only one end-segment distribution function, $q_\beta(\mathbf{r},s)$, is needed, and the equation of $q_\beta(\mathbf{r},s)$ is similar to Eq. (1) with the initial condition, $q_\beta(\mathbf{r},0)=1$, and the boundary condition, $q_\beta(\mathbf{r}=\mathbf{r}_c,s)=0$.

The individual canonical partition function of the grafted chains (α chains) subject to the mean field w_α is defined as Q_α. In terms of q_α and $q_\alpha^\dagger$, it can be written as

$$Q_\alpha=\int d\mathbf{r}\; q_\alpha(\mathbf{r},s)q_\alpha^\dagger(\mathbf{r},s). \tag{2}$$

Note that Q_α is independent of the parameter s. The expression for Q_β is similar

$$Q_\beta=\int d\mathbf{r}\; q_\beta(\mathbf{r},s)q_\beta(\mathbf{r},P-s). \tag{3}$$

With the mean field approximation, the free energy of the system is given by

$$\frac{\mathcal{F}}{\rho_0 k_B T}=-n_\alpha\rho_0^{-1}\ln\frac{Q_\alpha}{n_\alpha\rho_0^{-1}}-n_\beta\rho_0^{-1}\ln\frac{Q_\beta}{n_\beta\rho_0^{-1}}+\int d\mathbf{r}[-w_\alpha\psi_\alpha-w_\beta\psi_\beta-\xi(1-\psi_\alpha-\psi_\beta)], \tag{4}$$

where k_B is the Boltzmann constant, T is the temperature, $\psi_\alpha(\mathbf{r})$ is the local volume fraction of the grafted chains, $\psi_\beta(\mathbf{r})$ is the local volume fraction of the free chains, and $\xi(\mathbf{r})$ is the potential field that ensures the incompressibility of the system.

Minimizing the free energy in Eq. (4) with respect to ψ_α, ψ_β, w_α, w_β, and ξ leads to the following mean field equations that describe the equilibrium morphology:[13,17,18]

$$w_\alpha(\mathbf{r})=\xi(\mathbf{r}), \tag{5}$$

$$w_\beta(\mathbf{r})=\xi(\mathbf{r}), \tag{6}$$

$$\psi_\alpha(\mathbf{r})+\psi_\beta(\mathbf{r})=1, \tag{7}$$

$$\psi_\alpha(\mathbf{r})=\frac{n_\alpha\rho_0^{-1}}{Q_\alpha}\int_0^N ds\; q_\alpha(\mathbf{r},s)q_\alpha^\dagger(\mathbf{r},s), \tag{8}$$

$$\psi_\beta(\mathbf{r})=\frac{n_\beta\rho_0^{-1}}{Q_\beta}\int_0^P ds\; q_\beta(\mathbf{r},s)q_\beta(\mathbf{r},P-s). \tag{9}$$

In general, Eqs. (5)–(9) must be solved numerically. We choose to use the real space combinatorial screening algorithm of Drolet and Fredrickson to numerically solve Eqs. (5)–(9).[19,21] The calculations are carried out on a two-dimensional $L_x\times L_z$ lattice with periodic boundary condition. The size of the lattice is chosen such that $L_x=L_z\gg aN^{1/2}$ to avoid finite size effect.[22] To simplify the system and the calculation, we assume equal polymerization indexes of the grafted chains and the free chains; that is, we take $N=P$, the system is in the long solvent regime. The algorithm then consists of generating the initial values of the fields. Using a Crank–Nicholson scheme and an alternating-direction implicit (ADI) method,[23] the diffusion equations are then integrated to obtain q_α (q_β) and $q_\alpha^\dagger$, for $0\leqslant s\leqslant N(P)$. Next, the right-hand sides of Eqs. (8) and (9) are evaluated to obtain new expressions for the species volume fractions and the incompressibility field is chosen to be

$$\xi(\mathbf{r})=\xi(1-\psi_\alpha(\mathbf{r})-\psi_\beta(\mathbf{r})) \tag{10}$$

with ξ a constant with a high enough value to ensure that in practice $\psi_\alpha(\mathbf{r})+\psi_\beta(\mathbf{r})=1$ and that the resulting density profiles and energies are independent of its particular value.[13] The final step is to update the potential fields using Eqs. (5), (6), and (10) by means of a linear mix of new and old solutions. These steps are repeated until the (relative) free energy changes at each iteration are reduced to 10^{-4}. For the details of the calculation procedure, see Appendices A and B.

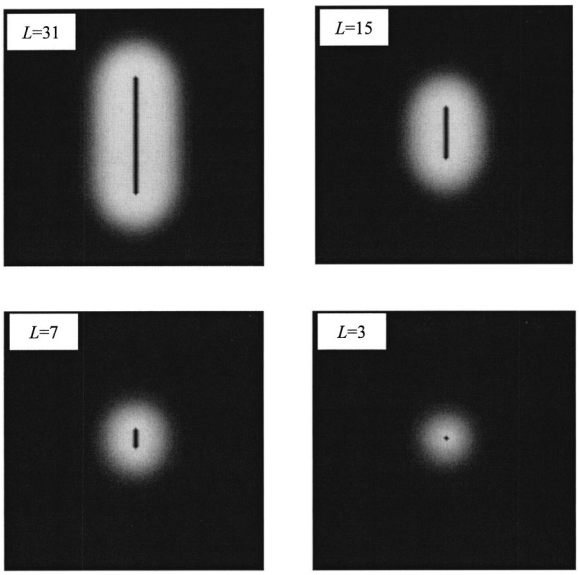

FIG. 2. Distribution of total monomer density of the grafted chains with $N=P=50$, $\sigma=0.25$ for different sheet lengths. The monomer density in the white region is higher than that in the dark region and the dark rectangles with different lengths in the center of the white region represent the clay sheets.

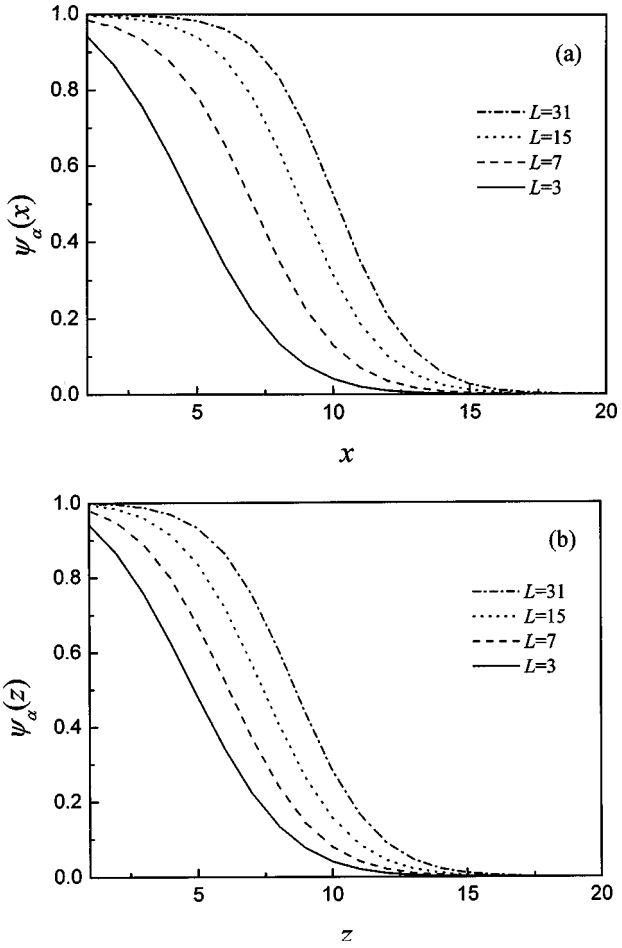

FIG. 3. Profiles of total monomer density of the grafted chains with $N=P=50$, $\sigma=0.25$ along (a) the x direction and (b) the z direction.

III. RESULTS AND DISCUSSION

A. Morphology

We first illustrate how the brush structures change with various sheet lengths L. For clarity, only one clay sheet grafted with polymer chains is considered here. The distributions of the monomer density for $N=50$ and $\sigma=0.25$ with different lateral lengths of the clay sheet, L, are shown in Fig. 2. These distributions demonstrate the large influence of the lateral length of the clay sheet on the structure of the grafted chain layer. The shape of the monomer density distribution varies smoothly from what appears to be an ellipse when $L \gtrsim aN^{1/2}$ to a circle when $L \lesssim aN^{1/2}$.

The corresponding monomer density profiles along the x and z directions are shown in Figs. 3(a) and 3(b), respectively. When $L \gtrsim aN^{1/2}$, in both directions the shape of the monomer density profiles is the parabolic, which is characteristic of polymer brushes at a flat interface; when $L \lesssim aN^{1/2}$, the shape of the density profile is the power law decay in both the x- and z-directions, which is typical of a star polymer.[24] Similar behavior has been observed in a system of polymer chains grafted to a spherical interface.[25] In that case, by changing the core curvature and using a modified Derjaguin approximation, the grafted layer assumes structures ranging from those in star polymer systems to planar polymer brushes. In the present 2D calculation, without any further approximation, similar structures are predicted by changing the lateral length of the clay sheets.

The interaction between the two polymer brushes also alters the structure of the brushes. As an example, we first illustrate in Fig. 4 the distribution of the monomer density for two clay sheets with $L=31$ and each surface grafted with $N=50$ chains at different distances H. For convenience, the surface of each sheet facing another approaching sheet will be called front surface and the other rear surface, and the brushes grafted on the front and rear surfaces are named the front and rear brushes, respectively. For the values of $\sigma(=0.25)$ and $P(=50)$ used, the systems are well in the "dry" brush regime (where $\sigma N^{1/2} \gtrsim 1$). The brush height is roughly equal to the predicted value, $h \simeq aN\sigma \simeq 12$. When $H \gg 2h$, i.e., the two clay sheets are far away from each other and no interaction exists between the two front brushes, the melt polymer chains penetrate into the space between the tails of the two separated front brushes, and one finds that the monomer density of the grafted chains are almost zero in this area. As the distance between the sheets decreases and reaches a critical value defined by $H^* \simeq 2h$, the tails of the two front brushes start to touch each other and the area in which the monomer density of the front brushes equal zero disappears, i.e., the melt chains being expelling out from this area. If the distance of the two sheets is further decreased ($H \ll 2h$), one can see that almost all the free chains are expelled out of the front brushes. The density profile of the rear brushes remains almost unchanged as the two sheets move closer.

Figure 5 shows the distributions of the monomer density for sheet length $L=W=3$ and $N=50$. In this extreme case, where L, $W \lesssim aN^{1/2}$, the distributions of the monomer of the polymer layers resemble that of star polymers and the layer thickness is predicted as $h \simeq aN^{1/2} \simeq 7$. Although the distance between the sheets reaches the critical value that the tails of the two front layers start to touch each other, the melt chains are not completely expelled out from this area. Decreasing the distance further, one finds that all the free chains are expelled out from the front layers.

B. Interactions

The interaction free energy for the two brushes at a distance H is given by[13]

$$\frac{\mathcal{F}(H)}{\rho_0 k_B T} = -n_\alpha \rho_0^{-1} \ln \frac{Q_\alpha}{n_\alpha \rho_0^{-1}} - \int d\mathbf{r}\, w_\alpha \psi_\alpha \tag{11}$$

and the free energy difference

$$\frac{F(H)}{\rho_0 k_B T} = \mathcal{F}(H) - \mathcal{F}(\infty), \tag{12}$$

where the reference state is taken to be the state where the two clay sheets are separated far enough so that they do not feel each other, i.e., the monomer density distributions of the two brushes are not altered even when one separates them further. In Fig. 6 we present the results obtained for the interaction free energy $F/\rho_0 k_B T$ of the two brushes ($N=50$) in a melt ($P=50$) as a function of the distance H between them, for different values of the grafting density σ. The four curves plotted in Fig. 6 correspond to the four values of the grafting

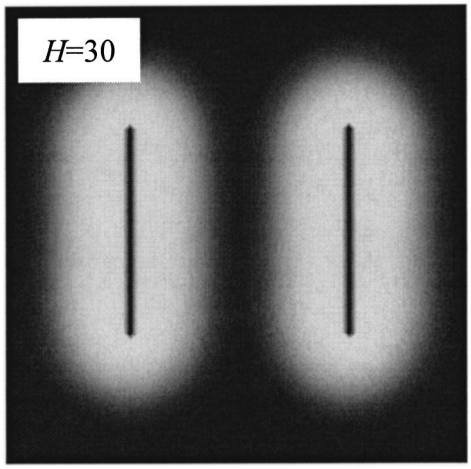

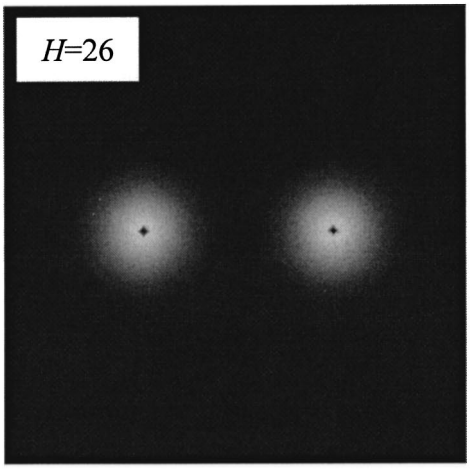

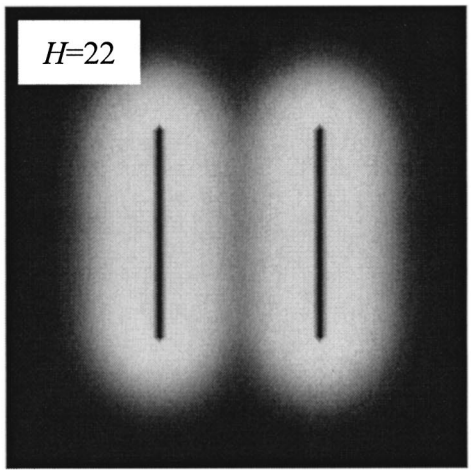

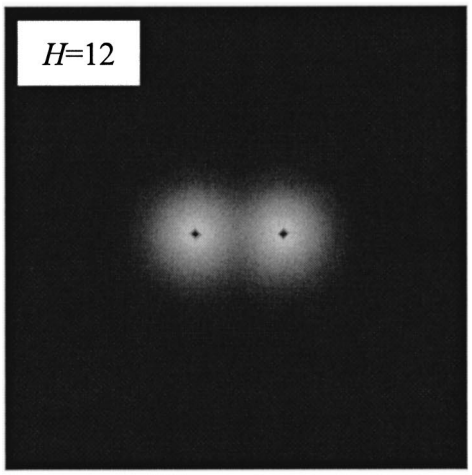

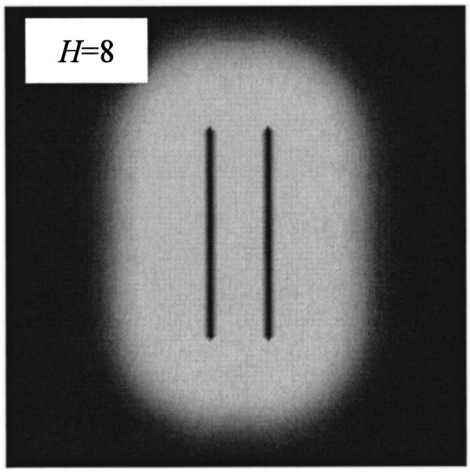

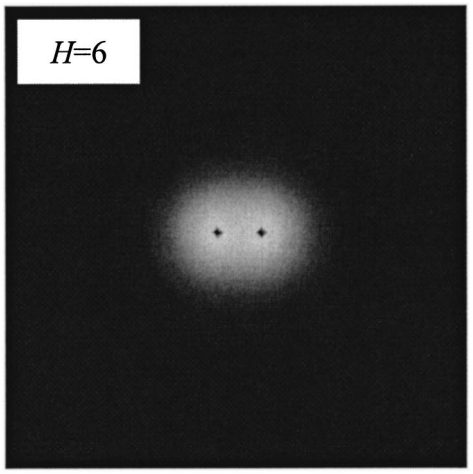

FIG. 4. Distribution of total monomer density of the grafted chains with $N=P=50$, $\sigma=0.25$ and $L=31$, $W=3$ at different distances. The monomer density in the white region is higher than that in the dark region and the dark rectangles with different lengths in the center of the white region represent the clay sheets.

FIG. 5. Distribution of total monomer density of the grafted chains with $N=P=50$, $\sigma=0.25$ and $L=3$, $W=3$ at different distances. The monomer density in the white region is higher than that in the dark region and the dark rectangles with different lengths in the center of the white region represent the clay sheets.

density for $N=P=50$, $L=31$ at $\sigma=0.039$ (stars), $\sigma=0.117$ (triangles), $\sigma=0.156$ (circles), and $\sigma=0.195$ (squares). At small brush separation there is a repulsive part in the interaction free energy for all four cases due to the excluded volume effect between the grafted polymers, while at large brush separations there is no interaction between the brushes. At intermediate distances (roughly at the contact distances of the tails of the two brushes) and for relatively high

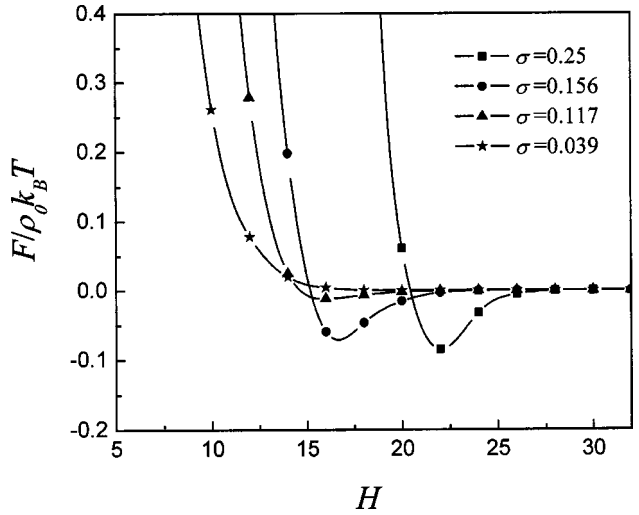

FIG. 6. Free energy of interaction of two brushes as a function of the distance between the two front surfaces with $N=P=50$, $L=31$, $W=3$ for different values of the grafting density: $\sigma=0.039$ (stars), $\sigma=0.117$ (triangles), $\sigma=0.156$ (circles), and $\sigma=0.25$ (squares). The symbols are obtained for the numerical calculations and the solid curves are the fits to the symbols.

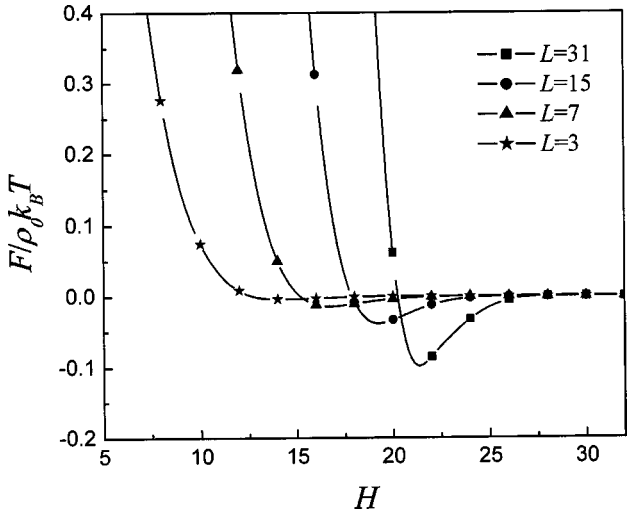

FIG. 7. Free energy of interaction of two brushes as a function of the distance between the two front surfaces with $N=P=50$, $\sigma=0.25$, $W=3$ for different values of the lateral length: $L=3$ (stars), $L=7$ (triangles), $L=15$ (circles), and $L=31$ (squares). The symbols are obtained from the numerical calculations and the solid curves are the fits to the symbols.

grafting densities [$\sigma N^{1/2} \gtrsim (N/P)^{3/2}$], however, it is surprising to see that the interactions are attractive. The reason for the appearance of the attractive interactions for polymer brushes immersed in a chemically identical polymer melt was explained by Leibler *et al.* and Gay as follows.[11,12] Once the brush and the melt are in contact, they adjust the penetration length λ so as to minimize the overall interfacial free energy. The extra stretching of the brush, when the interface is broadened over the width λ, contributes to the interfacial energy as $\mathcal{F}_{\text{brush}} \simeq k_B T \sigma \lambda^2 / N a^4$.[11,26] The contribution of the melt component to the interfacial energy, $\mathcal{F}_{\text{melt}}$, however, scales differently for different melt chain (free chain) lengths. For a melt of short chains ($P<P^*$, where $P^* = N^{2/3}\sigma^{-2/3}$ is a crossover polymerization index predicted by Leibler *et al.* and Gay), it scales as $\mathcal{F}_{\text{melt}} \simeq -k_B T \lambda / P a^3$, which comes from the contribution from the translational entropy of the solvent since in this case the melt chains can be considered as pointlike objects ($aP^{1/2} \ll \lambda$). On the other hand, for a melt of longer chains ($P>P^*$), the melt interfacial energy scales as $\mathcal{F}_{\text{melt}} \simeq k_B T / \lambda a$, which is positive and accounts for the fact that when the interface width is smaller than the typical extension of the solvent molecules ($\lambda \ll aP^{1/2}$), many conformation of the free chains (those that would cross the interface) are forbidden near the interface. Therefore, in this case, the decrease of the distance between the brushes causes a progressive expulsion of the free chains and gives rise to an increasingly negative energy of interaction. The minimum is attained when the two brushes start to compress each other and a positive repulsive contribution to the energy appears. Indeed, our calculation agrees with the scaling predictions of Leibler *et al.* and Gay fairly well. For $\sigma=0.25$ (squares) and $\sigma=0.156$ (circles), in which $\sigma N^{1/2} > (N/P)^{3/2}$, it is seen that the interactions are attractive, while for $\sigma=0.039$ (stars), where $\sigma N^{1/2} < (N/P)^{3/2}$, the interaction is purely repulsive.

In the arguments of Leibler *et al.* and Gay, the lateral length of the brushes is assumed to be infinitively long ($L \to \infty$) and is thus not considered to be a relevant length scale. Our 2D SCF calculation reveals, however, it is not the case. Figure 7 shows the interaction free energy of the two brushes with different L and fixed grafting density σ in the regime ($P>P^*$). It is seen that for $L/aN^{1/2} \gg 1$, at intermediate distances the interactions are attractive, which is similar to that in Fig. 6 with $P>P^*$; however, as for $L/aN^{1/2} \ll 1$ ($L=3$, the stars in Fig. 7), the interaction is purely repulsive. In fact, as L, $W \ll aN^{1/2}$, the structure of the grafted layers appears like that of star polymers. Witten and Pincus considered the stabilization of extra-small colloidal particles grafted by polymer chains.[27] Using scaling argument, they showed that for long chain and high grafting density the grafted layers experience purely repulsive force, which is in agreement with the present 2D SCF calculation. Therefore, our 2D SCF calculation shows that the lateral length of the clay sheets is indeed a new relevant length scale in the problem we considered here. Decreasing the lateral length of the clay sheets can cause a substantial change in the interacting force between the clay sheets. The appearance of the attractive interaction can either be caused by increasing the grafting density or by increasing the lateral length of the clay sheets.

We calculate in a systematic way the locus of points N, P, L, and σ at which the attractive interaction disappears. For fixed value of N, P, and L, the grafting density was varied until the first value of σ, for which the free energy of interaction becomes negative, was found. The free energy was computed with accuracy to four decimal places and in some cases a few thousand iterations of the set of equations were necessary in order to attain the desired precision. The results obtained for $N=P=30$ (filled circles) and $N=P=50$ (squares) are shown in Fig. 8. Also shown in the same figure is the curve corresponding to the scaling function

$$\sigma N^{1/2} = f_1(L/aN^{1/2}) \tag{13}$$

with

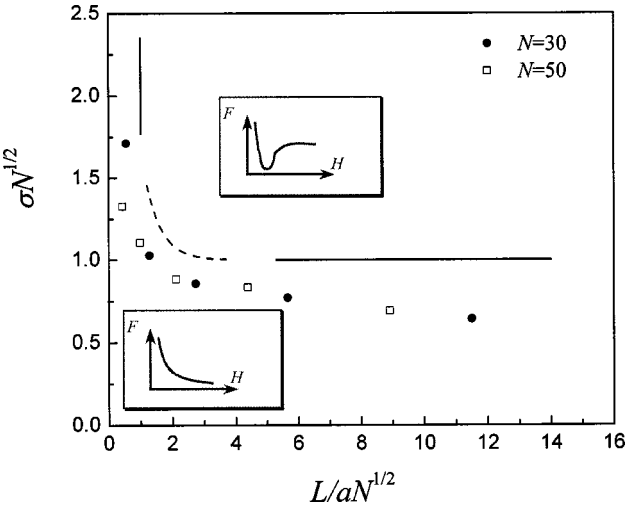

FIG. 8. Locus of points (N, σ, L) that characterize the beginning of the expulsive of the mobile chains from the grafted layer. Results are presented for $N=P=30$ (filled circles) and $N=P=50$ (squares). The solid and dashed curves are the sketch of the proposed scaling function defined in Eq. (14). The upper cartoon denotes an interaction with an attractive part and the lower one denotes a purely repulsive interaction.

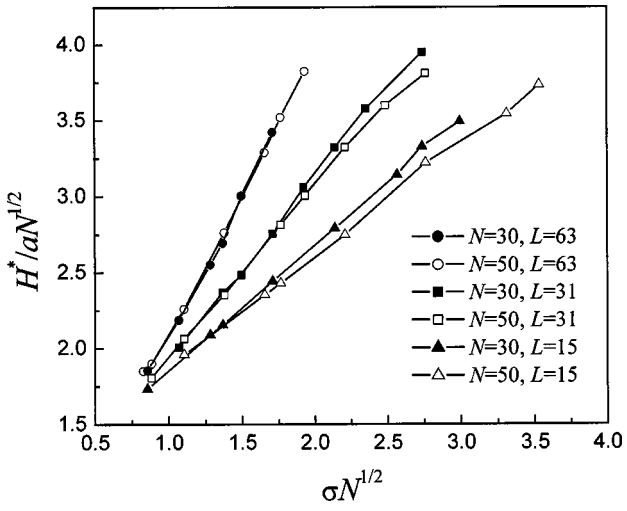

FIG. 9. The position of the minimum of the interaction free energy as a function of the polymerization indexes of the grafted and melt chains, N and P, the lateral length of the clay sheets, L, and the grafting density, σ.

$$f_1(X)=\begin{cases}1, & X\gg 1,\\ \infty, & X\ll 1,\end{cases} \tag{14}$$

where $X=L/aN^{1/2}$. The scaling function is proposed based on the following observations. In the $L/aN^{1/2}\gg 1$ limit, the structure of the grafted layer is that of a polymer brush at an infinitely long, flat interface, in which case scaling arguments by de Gennes and Gay show that the beginning of the expulsion of the mobile chains from the grafted layer occurs when $\sigma N^{1/2}>(N/P)^{3/2}$;[8,12] while in the $L/aN^{1/2}\ll 1$ limit, the structure of the grafted layer is that of a star polymer, in which case the scaling argument by Witten and Pincus and experiments and simulations by Likos *et al.* show that the interactions between two star polymers are purely repulsive.[27,28] The general trends of our data are well represented by the scaling prediction.

In Fig. 9 we present the results obtained for the distances for which the minimum of the interaction is attained for various values of N, P, σ, and L. Since the effective attraction between the brushes results from the replacement of two unfavorable brush–melt interfaces by a single brush–brush interface, the distance at which the attraction attains its maximum value is roughly the sum of the two equilibrium heights of the brushes, i.e.,

$$H^*\simeq 2h\simeq 2aN\sigma. \tag{15}$$

Indeed, it is seen from Fig. 9 that all the curves are straight lines. However, the slopes of the lines appear to be dependent on the value of $L/aN^{1/2}$. For the cases with $L=63$, $N=30$ (filled circles), and $N=50$ (open circles), all the data points fall onto one line and the slope of the line is equal to 2, in accordance with Eq. (15), which means that for $L/aN^{1/2}\gg 1$ the lateral length is not relevant in determining the peak position. However, decreasing the value of $L/aN^{1/2}$ decreases the slope of the lines, which means that in the intermediate regime ($L\sim aN^{1/2}$), the lateral length of the clay sheets is relevant and the peak position is affected by this length scale.

Finally, the minimum of the attractive energy varies with the values of N, P, σ, and L. In Fig. 10, it is seen that for small $L/aN^{1/2}$ values ($L/aN^{1/2}\sim 1$), $|F_{\min}|/\rho_0 k_B TL$ increases with the increase of $L/aN^{1/2}$, while for large $L/aN^{1/2}$ values ($L/aN^{1/2}\gg 1$), $|F_{\min}|/\rho_0 k_B TL$ appears to saturate at different values for different grafted and melt chains, which is reasonable: for an infinitively long sheet, the attractive energy per unit length is independent of its lateral length.[29] The asymptotic behavior of the energy in L cannot be described by the existing scaling theory.

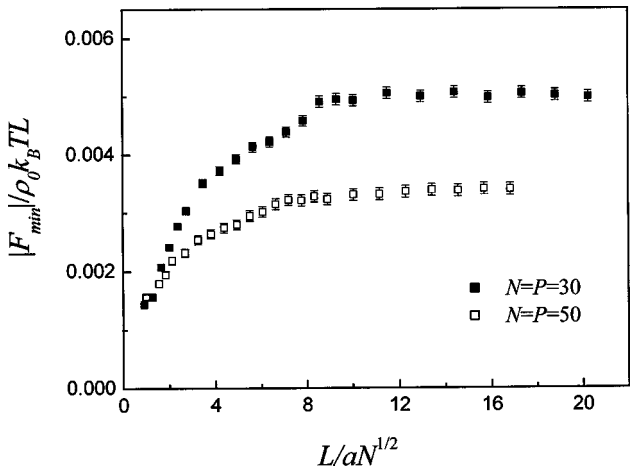

FIG. 10. Absolute value of the minimum of the interaction free energy of two brushes at a fixed grafting density ($\sigma=0.25$) with $N=P=30$ (filled squares) and $N=P=50$ (squares) as a function of the lateral length of the clay sheets, L. For each data point, three independent runs starting with different initial (random) states were carried out to estimate the typical error of the free energy difference calculation and the error bars were thus determined.

IV. CONCLUSION AND REMARKS

We have used a 2D SCF algorithm to carry out a systematic analysis of two brush-coated clay sheets immersed in a polymer melt. One of the main findings of this article is that, in addition to the polymerization indexes of the grafted chains N, and the free chains P, and the grafting density σ, the lateral length of the clay sheets L is also a relevant length scale in the system we considered here. We have found that due to subtle entropic and elastic effects the interactions between the two grafted layers show an attractive part by varying either the grafting density σ or the lateral length of the clay sheets L at fixed polymerization indexes of the grafting chains N and the matrix (free) chains P. We have calculated the locus of points N, P, L, and σ at which the expulsion of the free chains from the grafted layers begins and the attractive interaction disappears. We have shown that the positive interfacial tension between the grafted and the free chains is responsible for the appearance of the attractive minimum in the interaction energy of two brushes immersed in a chemically identical polymer melt. These findings may have various implications for creating novel polymeric nanocomposites.

The present 2D SCF model bridges the gap between the existing models for brushes grafted on flat interface and stars of polymer chains tethered to a central microscopic core. Such a model would be useful to investigate the structure and phase diagrams of the experimental systems such as self-assembly of grafted nano-particles immersed in polymer matrix, colloidal stabilization in a polymer solution, and wetting of protected surfaces by polymeric materials. The essential features of these systems can be analyzed within the model presented here.

In our calculation, we have taken $N=P$, however, it is known from a 1D SCF calculation (in which the length scale of the inorganic particles is assumed to be much larger than that of the polymer chains grafted on them) that the interaction between the two brushes are profoundly influenced by the melt chain polymerization index, P.[13] Thus, it is interesting to see what will be the effect of the free chain polymerization index P in the regime of intermediate sheet lengths. Finally, we note that it is straightforward to extend the present model to other complicated yet still realistic situations, for example, if the grafted chains and the matrix chains are chemically different, either incompatible (with the Flory interaction parameter $\chi>0$) or attractive ($\chi<0$), the structure and interactions of the grafted layers are greatly influenced, as was shown by recent 1D SCF studies.[14,30] Another interesting example is to investigate the clay particles dispersed in a lamellar matrix composed of a block copolymer or a lyotropic smectic.[31,32] These works are currently underway.

ACKNOWLEDGMENTS

The authors gratefully acknowledge support from the Special Funds for Major State Basic Research Projects (G1999064800) and the National Natural Science Foundation of China through Grant No. 20104002. R.W. acknowledges the financial support of China Postdoctoral Science Foundation (2002031170).

APPENDIX A: THE SCF PROCEDURE

In this Appendix, we briefly describe our numerical method. First, we discretize the variables x, z and s as

$$\begin{aligned} x&=i\Delta x, \quad i=1,2,\ldots,L_x,\\ z&=j\Delta z, \quad j=1,2,\ldots,L_z,\\ s&=t\Delta s, \quad t=1,2,\ldots,M, \end{aligned} \tag{A1}$$

where L_x and L_z are lattice sizes along the x and z directions, respectively. Typically $\Delta x=\Delta z=1$, $\Delta s=1$, and M was chosen as $M=N$ when solving the diffusion equation of the α chains and $M=P$ for the β chains. The statistical length of the monomers, a, was set to be $a=1$ and the volume of the monomers $\rho_0^{-1}=1$. The SCF equations are solved on the 2D $L_x\times L_z$ lattice with periodic boundary condition. Our algorithm then comprises six steps which are described as follows [We write $q(\mathbf{r},s)$ as $q(i,j,t)$, other position dependent variables are written in a similar way.]

(1) Set the initial values of the potential fields $w_\alpha(i,j)$ and $w_\beta(i,j)$ using a random number generator. Set the initial value of the potential field $\xi(i,j)$ to $\xi(i,j)=1/2[w_\alpha(i,j)+w_\beta(i,j)]$.

(2) Solve the modified diffusion equations of $q_\alpha(i,j,t)$, $q_\alpha^\dagger(i,j,t)$ and $q_\beta(i,j,t)$ with the given initial and boundary conditions using the Crank–Nicholson method and the alternating-direction implicit (ADI) scheme (see Appendix B).

(3) Evaluate the monomer densities $\psi_\alpha(i,j)$ and $\psi_\beta(i,j)$ conjugated to $w_\alpha(i,j)$ and $w_\beta(i,j)$ using discrete versions of the Eqs. (8) and (9):

$$\psi_\alpha(i,j)=\frac{n_\alpha\rho_\alpha^{-1}}{Q_\alpha}\Delta s\sum_{t=0}^{N} q_\alpha(i,j,t)q_\alpha^\dagger(i,j,t), \tag{A2}$$

$$\psi_\beta(i,j)=\frac{n_\beta\rho_0^{-1}}{Q_\beta}\Delta s\sum_{t=0}^{P} q_\beta(i,j,t)q_\beta(i,j,P-t). \tag{A3}$$

(4) Update the potential fields $w_\alpha(i,j)$, $w_\beta(i,j)$, and $\xi(i,j)$ using the following descriptions:

$$w_\alpha^{\text{new}}(i,j)=w_\alpha^{\text{old}}(i,j)+\omega[\xi^{\text{old}}(i,j)-w_\alpha^{\text{old}}(i,j)], \tag{A4}$$

$$w_\beta^{\text{new}}(i,j)=w_\beta^{\text{old}}(i,j)+\omega[\xi^{\text{old}}(i,j)-w_\beta^{\text{old}}(i,j)], \tag{A5}$$

$$\xi^{\text{new}}(i,j)=\xi^{\text{old}}(i,j)+\xi[1-\psi_\alpha(i,j)-\psi_\beta(i,j)]. \tag{A6}$$

(5) Evaluate the free energy of the system using the following discrete version of the Eq. (4):

$$\begin{aligned} \frac{\mathcal{F}}{\rho_0 k_B T}=&-n_\alpha\rho_0^{-1}\ln\frac{Q_\alpha}{n_\alpha\rho_0^{-1}}-n_\beta\rho_0^{-1}\ln\frac{Q_\beta}{n_\beta\rho_0^{-1}}\\ &+a\Delta x\Delta z\sum_{i=1}^{L_x}\sum_{j=1}^{L_z}[-w_\alpha(i,j)\psi_\alpha(i,j)\\ &-w_\beta(i,j)\psi_\beta(i,j)-\xi(i,j)(1-\psi_\alpha(i,j)\\ &-\psi_\beta(i,j))], \end{aligned} \tag{A7}$$

where

$$Q_\alpha = a\Delta x\Delta z\sum_{i=1}^{L_x}\sum_{j=1}^{L_z} q_\alpha(i,j,t)q_\alpha^\dagger(i,j,t) \tag{A8}$$

and

$$Q_\beta = a\Delta x\Delta z\sum_{i=1}^{l_x}\sum_{j=1}^{L_z} q_\beta(i,j,t)q_\beta(i,j,P-t), \tag{A9}$$

Note that both Q_α and Q_β are independent of the parameter t.

(6) Return to step (2).

The iterative procedure continues until the (relative) free energy changes at each iteration are reduced to 10^{-4}. The relaxation parameter ω appearing in step (4) determines how fast the free energy converges to a local minimum. In the present article ω is set to be $\omega=0.1$. The parameter ξ is set to be $\xi=1.0$. As long as ξ is not small, the incompressibility condition, Eq. (7), is ensured and the resulting density profiles and free energies are independent of its particular value. Larger values of ω and ξ can speed up convergence but also may lead to numerical instabilities.

APPENDIX B: THE ADI SCHEME

We take the modified diffusion equation of $q_\alpha(i,j,t)$ [Eq. (1)] as an example. The discrete version of Eq. (1) is obtained by using the Crank–Nicholson method:[23]

$$\begin{aligned}\frac{q_\alpha(i,j,t)-q_\alpha(i,j,t-1)}{\Delta s} &= \frac{a^2}{12}[\nabla_x^2 q_\alpha(i,j,t)+\nabla_z^2 q_\alpha(i,j,t)\\ &\quad+\nabla_x^2 q_\alpha(i,j,t-1)+\nabla_z^2 q_\alpha(i,j,t-1)]-\frac{1}{2}w_\alpha(i,j)\\ &\quad\times[q_\alpha(i,j,t)+q_\alpha(i,j,t-1)].\end{aligned} \tag{B1}$$

The above equation is solved by the so-called alternating-direction implicit scheme.[23] The idea is to divide each timestep into two steps of size $\Delta s/2$. In each substep, a different direction is treated implicitly:

$$\begin{aligned}q_\alpha\left(i,j,t-\frac{1}{2}\right) &= q_\alpha(i,j,t-1)+\frac{a^2\Delta s}{12}\left[\nabla_x^2 q_\alpha\left(i,j,t-\frac{1}{2}\right)\right.\\ &\quad\left.+\nabla_z^2 q_\alpha(i,j,t-1)\right]-\frac{\Delta s}{4}w_\alpha(i,j)\\ &\quad\times\left[q_\alpha\left(i,j,t-\frac{1}{2}\right)+q_\alpha\left(i,j,t-1\right)\right],\end{aligned} \tag{B2}$$

$$\begin{aligned}q_\alpha(i,j,t) &= q_\alpha\left(i,j,t-\frac{1}{2}\right)+\frac{a^2\Delta s}{12}\left[\nabla_x^2 q_\alpha\left(i,j,t-\frac{1}{2}\right)\right.\\ &\quad\left.+\nabla_z^2 q_\alpha(i,j,t)\right]-\frac{\Delta s}{4}w_\alpha(i,j)\left[q_\alpha(i,j,t)\right.\\ &\quad\left.+q_\alpha\left(i,j,t-\frac{1}{2}\right)\right].\end{aligned} \tag{B3}$$

The second derivative $\nabla_x^2 q_\alpha(i,j,t)$ is defined as $\nabla_x^2 q_\alpha(i,j,t) = q_\alpha(i+1,j,t)+q_\alpha(i-1,j,t)-2q_\alpha(i,j,t)/(\Delta x)^2$ and $\nabla_z^2 q_\alpha(i,j,t)$ is defined in a similar way. After some algebra the above equations can be written into the following tridiagonal forms in i and j, respectively,

$$\begin{aligned}&Aq_\alpha(i-1,j,t-\tfrac{1}{2})+B(i,j)q_\alpha(i,j,t-\tfrac{1}{2})+Cq_\alpha(i+1,j,t-\tfrac{1}{2})\\ &\quad=D(i,j,t-1)\end{aligned} \tag{B4}$$

and

$$\begin{aligned}&Aq_\alpha(i,j-1,t)+B(i,j)q_\alpha(i,j,t)+Cq_\alpha(i,j+1,t)\\ &\quad=D'(i,j,t-\tfrac{1}{2}).\end{aligned} \tag{B5}$$

With the given initial and boundary conditions, the tridiagonal matrices are solved to obtain $q_\alpha(i,j,t)$. The diffusion equations of $q_\alpha^\dagger(i,j,t)$ and $q_\beta(i,j,t)$ can be solved similarly.

[1] E. P. Giannelis, R. K. Krishnamoorti, and E. Manias, Adv. Polym. Sci. **138**, 107 (1999) and references therein.
[2] K. Yano, A. Uzuki, A. Okada *et al.*, J. Polym. Sci., Part A: Polym. Chem. **31**, 2493 (1993).
[3] E. Manias, A. Touny, L. Wu *et al.*, Chem. Mater. **13**, 3516 (2001).
[4] R. A. Vaia, S. Vasudevan, W. Krawiec *et al.*, Adv. Mater. **7**, 154 (1995).
[5] P. Liu, K. Gong, P. Xiao *et al.*, Mater. Chem. **10**, 933 (2000).
[6] M. G. Kanatzidis, L. M. Tonge, and T. J. Marks, J. Am. Chem. Soc. **109**, 3797 (1987).
[7] S. Alexander, J. Phys. (France) **38**, 983 (1977).
[8] P. G. de Gennes, Macromolecules **13**, 1069 (1980).
[9] P. G. de Gennes, *Scaling Concepts in Polymer Physics* (Cornell University Press, New York, 1985), Chap. 2.
[10] M. Aubouy, G. H. Fredrickson, P. Pincus *et al.*, Macromolecules **28**, 2979 (1995).
[11] L. Leibler, A. Ajdari, A. Mourran *et al.*, in *Ordering in Macromolecular Systems*, edited by A. Teramoto, M. Kobayashi, and T. Norisuji (Springer Verlag, Berlin, 1994).
[12] C. Gay, Macromolecules **30**, 5939 (1997).
[13] P. G. Ferreira, A. Ajdari, and L. Leibler, Macromolecules **31**, 3994 (1998).
[14] A. C. Balazs, C. Singh, and E. Zhulina, Macromolecules **31**, 8370 (1998).
[15] S. F. Edwards, Proc. Phys. Soc. **85**, 613 (1965).
[16] E. Helfand, J. Chem. Phys. **62**, 999 (1975).
[17] K. M. Hong and J. Noolandi, Macromolecules **14**, 727 (1981).
[18] M. W. Matsen and M. Schick, Phys. Rev. Lett. **72**, 2660 (1994).
[19] F. Drolet and G. H. Fredrickson, Phys. Rev. Lett. **83**, 4317 (1999).
[20] A. K. Dolan and S. F. Edwards, Proc. R. Soc. London, Ser. A **337**, 509 (1974).
[21] F. Drolet and G. H. Fredrickson, Macromolecules **34**, 5317 (2001).
[22] Due to the symmetry of the specific model we discussed in the present article, in the mean field approximation, the calculation needs only to be done in the lattice $(L_x/2)\times(L_z/2)$ with appropriate boundary conditions. That will speed up the cpu time by a factor of 4. Our codes are, however, developed for more general cases, thus, we have carried out the calculation in the full lattice. We have also verified that the monomer density of the P melt chains reaches a constant $\psi_\beta=1$ at the boundaries of the system, i.e., the P chains attain their bulk properties at the boundaries. Therefore the use of periodic boundary condition is appropriate and convenient.
[23] W. H. Press, B. P. Flannery, S. A. Teukolsky, and W. T. Vetterling, *Numerical Recipes* (Cambridge University Press, Cambridge, England, 1989).
[24] As $L \lesssim aN^{1/2}$, the structure in 3D is actually that of a *bottle brush polymer* due to the translational invariance along the y-direction. In a plane normal to the y-direction, however, the structure resembles a two-dimensional *star polymer* and it is in this sense that we use the term star polymer.
[25] E. K. Lin and A. P. Gast, Macromolecules **29**, 390 (1996).
[26] A. N. Semenov, Macromolecules **25**, 4967 (1992).
[27] T. A. Witten and P. A. Pincus, Macromolecules **19**, 2509 (1986).
[28] C. N. Likos, H. Lowen, M. Watzlawek *et al.*, Phys. Rev. Lett. **80**, 4450 (1998).
[29] In principle the SCF method excludes fluctuations. The solution of the self-consistent equations should be independent of the boundary and initial conditions. Indeed,the fluctuations of the density profiles [$\psi_\alpha(\mathbf{r})$ and $\psi_\beta(\mathbf{r})$] and free energy [$\mathcal{F}(H)/\rho_0 k_B TL$] in our numerical calculation are

negligible (relative error $>0.01\%$). The higher relative error of the free energy difference $F_{\min}/\rho_0 k_B TL(\sim 3\%)$ is because the values of $\mathcal{F}_{\min}/\rho_0 k_B TL$ and $\mathcal{F}_{\infty}/\rho_0 k_B TL$ are too close. It is difficult to reduce this kind of error in a SCF numerical calculation.

[30] I. Borokhov and L. Leibler, Macromolecules **35**, 5171 (2002).
[31] J. Groenewold and G. H. Fredrickson, Eur. Phys. J. B **5**, 171 (2001).
[32] R. B. Thompson, V. V. Ginzburg, M. W. Matsen, and A. C. Balazs, Macromolecules **35**, 1060 (2002).